MECSOL 2019 - Proceedings of the 7th International Symposium on Solid Mechanics
V. Tita, A. Ferreira, M.L. Ribeiro, A. Vieira and A.T. Beck (Editors), ABCM, Sao Carlos, SP, Brazil, April 15th to 17th, 2019

Fatigue-Driven Delamination Modelling Using a Linear-Polynomial Traction-Separation Law

Lucas A. Oliveira and Maurício V. Donadon

A path independent integral and the approximate analysis of stress concentration by notches and cracks ITA, Technological Institute of Aeronautics, Department of Aeronautical Engineering, São José dos Campos, Brazil

A constitutive damage model is proposed to predict static and high cycle fatigue-induced damage in carbon/epoxy composite laminates. This model accounts for fatigue-induced delamination in modes I, II and III either individually or combined without knowing the modes ratios a priori. The proposed formulation uses the linear-polynomial traction-separation law. The model estimates the strain energy release rate by using the J-integral method applied on the cohesive zone boundary. An algorithm identifies the elements in which the damage may nucleates and the elements at the crack front. The proposed formulation is implemented into ABAQUS/Explicit FE code within solid elements. The local part (at element level) of the algorithm is implemented in a user-defined material subroutine (VUMAT) and the non-local part (at structure level), in a VEXTERNALDB subroutine.
Keywords: Damage Mechanics, Fracture Mechanics, Fatigue, Finite Elements

INTRODUCTION

The transportation industry faces the challenge to provide products that combine high safety requirements, quality, comfort and good design with the low fuel burn in order to reduce the operational cost of their customers. In this context, the aerospace industry is expanding the application of composite materials from simple fairings, wardrobes and radomes to primary structural components such as fuselage and wings structures.

Fatigue-induced delamination is one of the possible failure modes when using laminated composite materials. Therefore, applying composite materials in primary structural elements of aircraft requires the development of numerical methods to predict failure modes in operational scenarios to improve the design of damage tolerant composite structures.

The constitutive law used in this model to represent the behaviour of the interface between two adjacent layers is based on the Cohesive Zone Model (CZM) and has the form of a linear-polynomial traction–separation law (TSL). The advantage of this law over the common used bi-linear law (Turon et al., 2007) is that it is numerically more stable due to its smoothness on both damage onset and fully failed displacement (Donadon et al., 2009). In Donadon and Lauda (2015), the model was extended to include Robinson et al. (2005) fatigue model. In this research, it was modified to include the proposed fatigue-induced damage model.

DAMAGE MODEL FORMULATION

The traction-separation relationship between two adjacent layers is based on the Cohesive Zone Model (CZM), as given by Eq. (1).

$$\begin{aligned}\sigma_I &= K_I(1-D_K)\langle\delta_I\rangle - K_I\langle-\delta_I\rangle\\ \sigma_{II} &= K_{II}(1-D_K)\delta_{II}\\ \sigma_{III} &= K_{III}(1-D_K)\delta_{III}\end{aligned} \tag{1}$$

where the subscript I, II, III refers to the pure modes direction ($I = 33$, $II = 13$, $III = 23$), σ is the stress acting on the interface, K is the interface stiffness, δ is the relative displacement of the two adjacent layers, $\langle\cdot\rangle = \max(\cdot, 0)$ is the Macaulay brackets, and the single damage variable D_K describes the material loss of stiffness for the three fracture modes. This damage variable is defined by Eq. (2).

$$D_K \equiv 1 - \frac{\tilde{K}}{K} \tag{2}$$

where $\tilde{\cdot}$ express the residual value. In fatigue analysis, is useful describes the damage in terms of area A. For this purpose, the damage variable D_A is defined.

$$D_A \equiv \frac{A^d}{A} = 1 - \frac{\tilde{A}}{A} \tag{3}$$

where the superscript d refers to the damaged value. The relationship between the damage variables D_K and D_A is given by:

$$D_K = 1 - \frac{\delta^0}{\delta^*}(1 - D_A) \tag{4}$$

were δ^0 is the damage onset displacement and δ^* is the displacement related to the current quasi-static damage, which will be detailed in the next section. The variable D_A is composed of two damage parameters simultaneously computed, namely quasi-static damage parameter D_A^s and fatigue damage parameter D_A^f.

$$D_A = D_A^s + D_A^f \tag{5}$$

STATIC DAMAGE EVOLUTION LAW

The linear-polynomial TSL combines two behaviours shown in Fig. 1. First, starting from zero displacement the material presents a linear elastic response until the stress reaches the strength limit value S at the damage onset displacement δ^0. After this point, the behaviour consists of a cubic polynomial softening response, which is representative of an averaged damage. In this cubic curve, the stress starts at the onset point with a zero derivative ($\frac{d\sigma}{d\delta}\,|_{\delta^0} = 0$) and decreases to zero at the fully failed displacement δ^f also ending with derivative equals to zero ($\frac{d\sigma}{d\delta}\,|_{\delta^f} = 0$). This zero derivatives imposed to the polynomial is the reason for the better numerically stability. After the fully failed displacement, the stress (and the stiffness) remains zero, and the material can no longer sustain loads.

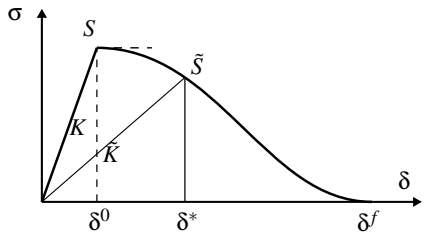

Figura 1 – Linear-polynomial TSL for a generic mode loading

From the smoothness conditions stated above, the residual strength is expressed as Eq. (6).

$$\tilde{S} = S\left(1 - \kappa^2(2\kappa - 3)\right) \tag{6}$$

with,

$$\kappa = \frac{\delta^* - \delta^o}{\delta^f - \delta^o} \tag{7}$$

Therefore, the area-based static damage variable D_A^s is given by,

$$D_A^s = \begin{cases} 0 & \text{if } \delta^* \leqslant \delta^0 \\ \kappa^2(2\kappa - 3) & \text{if } \delta^0 < \delta^* < \delta^f \\ 1 & \text{if } \delta^* \geqslant \delta^f \end{cases} \tag{8}$$

Since the damage is irreversible, the damage variable D_A^s is not allowed to decrease during unloading. can during increments. Furthermore, to express the stiffness damage parameter D_K as function of area damage variable D_A, as in

Eq. (4), the displacement δ^* is found from Eqs. (7) and (8). The solution of Eq. (8) for κ results in three different equations, as given by Eq. (9) and depicted in Fig. 2.

$$\kappa_{[1]} = \frac{1}{2} + \frac{1}{2}\left(\frac{1}{\lambda} + \lambda\right) \tag{9a}$$

$$\kappa_{[2]} = \frac{1}{2} - \frac{1}{4}\left(\frac{1}{\lambda} + \lambda\right) + \frac{\sqrt{3}}{4}\left(\frac{1}{\lambda} - \lambda\right) i \tag{9b}$$

$$\kappa_{[3]} = \frac{1}{2} - \frac{1}{4}\left(\frac{1}{\lambda} + \lambda\right) - \frac{\sqrt{3}}{4}\left(\frac{1}{\lambda} - \lambda\right) i \tag{9c}$$

where i is the imaginary unit ($i = \sqrt{-1}$) and,

$$\lambda = \left(1 - 2D_A^s + 2\sqrt{D_A^s(D_A^s - 1)}\right)^{1/3} \tag{10}$$

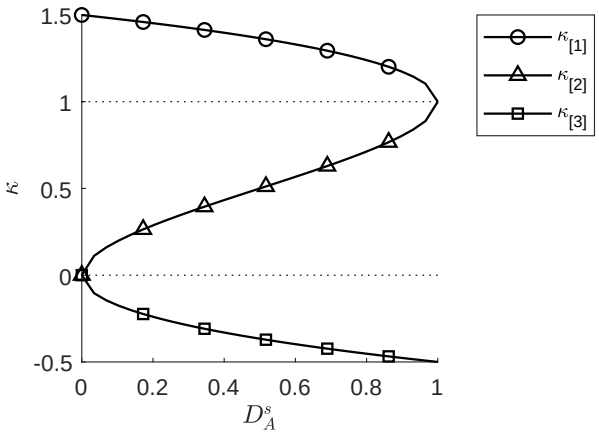

Figura 2 – Parameter κ as function of quasi-static damage D_A^s

Despite λ presents complex numbers as solution, the solution for $\kappa_{[1]}$, $\kappa_{[2]}$, and $\kappa_{[3]}$ are all real numbers. Furthermore, Fig. 2 shows that the second solution $\kappa_{[2]}$ presents the proper values going from $\kappa = 0$ at $D_A = 0$ to $\kappa = 1$ at $D_A = 1$. Therefore, from Eqs. (7) and (9b) the displacement δ^* associated to the current quasi-static damage is,

$$\delta^* = \delta^o + \left(\delta^f - \delta^o\right)\left[\frac{1}{2} - \frac{1}{4}\left(\frac{1}{\lambda} + \lambda\right) + \frac{\sqrt{3}}{4}\left(\frac{1}{\lambda} - \lambda\right) i\right] \tag{11}$$

The stiffness based damage variable is found from Eqs. (4), (5) and (11),

$$D_K = 1 - \frac{\delta^0}{\delta^o + \left(\delta^f - \delta^o\right)\left[\frac{1}{2} - \frac{1}{4}\left(\frac{1}{\lambda} + \lambda\right) + \frac{\sqrt{3}}{4}\left(\frac{1}{\lambda} - \lambda\right) i\right]}\left(1 - \left(D_A^s + D_A^f\right)\right) \tag{12}$$

Mixed Mode Delamination

The model described above can be applied to mixed mode delamination using an equivalent traction-displacement curve as represented in Fig. 3. In this equivalent curve, the equivalent displacement δ is obtained by Eq. (13).

$$\begin{aligned} \delta &= \sqrt{\langle \delta_I \rangle^2 + {\delta_s}^2} \\ \delta_s &= \sqrt{{\delta_{II}}^2 + {\delta_{III}}^2} \end{aligned} \tag{13}$$

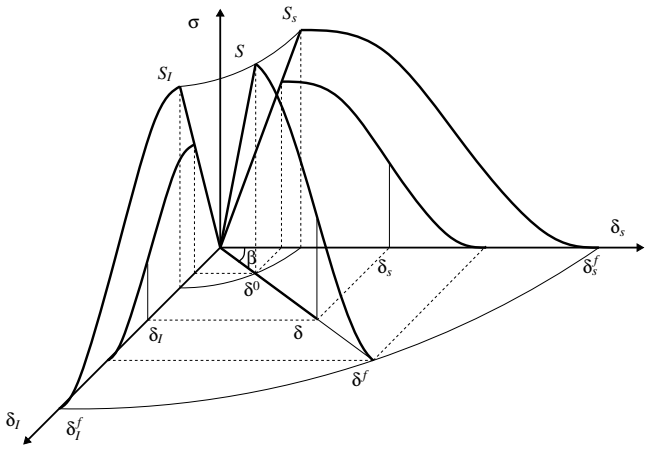

Figura 3 – Traction–separation for mixed mode delamination

where the subscript s refers to the combination of the two shear modes II and III. The equivalent damage onset displacement δ^0 is calculated employing a quadratic stress-based criterion (Ye, 1988).

$$\left(\frac{\langle\sigma_I\rangle}{S_I}\right)^2+\left(\frac{\sigma_s}{S_s}\right)^2=1 \tag{14}$$

Therefore, the equivalent damage onset displacement δ^0 is obtained by Eq. (15).

$$\delta^0=\left[\left(\frac{\langle K_I\cos(\beta)\rangle}{S_I}\right)^2+\left(\frac{K_s\sin(\beta)}{S_s}\right)^2\right]^{-\frac{1}{2}} \tag{15}$$

where $\cos\beta=\frac{\delta_s}{\delta}$. The fully damaged displacement δ^f is calculated using an energy-based the Power-Law criterion (Whitcomb et al., 1984).

$$\left(\frac{G_I}{G_{I,c}}\right)^\lambda+\left(\frac{G_s}{G_{s,c}}\right)^\lambda=1 \tag{16}$$

where G is the strain energy release rate (SERR) and G_c is the fracture toughness, with $G_s=G_{II}+G_{II}$ and $G_{s,c}=G_{II,c}=G_{III,c}$. Therefore, the equivalent fully damaged displacement δ^f is given by Eq. (17).

$$\delta^f=\frac{2}{\delta^0}\left[\left(\frac{K_I cos^2(\beta)}{G_{I,c}}\right)^\lambda+\left(\frac{K_s sin^2(\beta)}{G_{s,c}}\right)^\lambda\right]^{-\frac{1}{\lambda}} \tag{17}$$

FATIGUE DAMAGE EVOLUTION LAW

The fatigue-driven delamination is commonly described in terms of an effective main crack growth rate $\frac{da}{dn}$, which is measured through extensive tests and expressed by a Paris' law.

$$\frac{da}{dn}=C\left(\frac{\Delta G}{G_c}\right)^m \tag{18}$$

where ΔG is the SERR variation and the equation coefficient C and exponent m are experimentally determined fitting parameters.

Instead of degrading by fatigue the entire cohesive zone, the proposed model applies Eq. (18) only to the elements located at the crack-tip. For this purpose, the model uses a non-local tracking algorithm to identify the crack-tip elements, similarly to the way proposed by Kawashita and Hallett (2012). The algorithm works in two different stages. In the damage fatigue nucleation stage, it tracks the SERR peaks within the elements and set them as crack initiation elements. The fatigue propagation stage is characterised by the presence of at least one entirely failed element. In this case, the algorithm identifies the elements adjacent to a failed one.

The SERR cyclic variation ΔG is the difference between the maximum and minimum SERR achieved during the loading cycle, G_{max} and G_{min} respectively. Since representing the whole load spectrum in time is computationally expensive, only the maximum load level is computed following the envelope curve (Peerlings et al., 2000), shown in Fig. 4. The minimum load level is represented by the load ratio R and the SERR variation ΔG is calculated as given by Eq. (19).

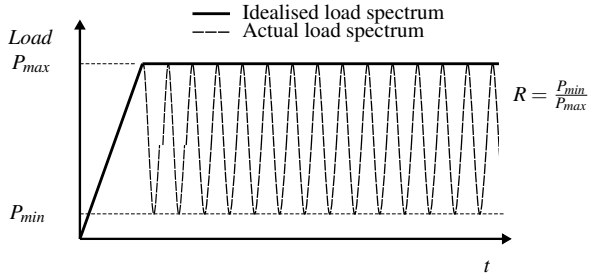

Figura 4 – Load spectrum idealisation

$$\Delta G = G_{max}\left(1 - R^2\right) \tag{19}$$

The maximum SERR is calculated by the J-integral, where the integration contour is taken at the cohesive elements surface, as shown in Fig. 5. The advantage of the J-integral over a time-integration approach is that for unloading event, the first present a more accurate estimation of the strain energy at the crack-tip.

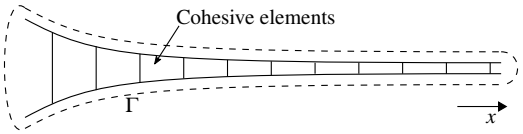

Figura 5 – Definition of the J-integral surrounding the cohesive zone.

$$G_{max} = J = J_I + J_{II} + J_{III} \tag{20}$$

where

$$J_j = \int_\Gamma \left(-\sigma_j \frac{\partial \delta_j}{\partial x}\right) \mathrm{d}\Gamma = \sum_k^{\text{element in } \Gamma} \left(-\frac{1}{2}\left(\sigma_j\left(x_k\right) + \sigma_j\left(x_{k+1}\right)\right)\left(\delta_j\left(x_{k+1}\right) - \delta_j(x_k)\right)\right) \tag{21}$$

where, $j = I, II, III$.

The increasing damage within the element reduces its stiffness, which causes the displacement to increase, even if the overall load is kept constant. This results in an increasing SERR estimation, that only reaches the correct imposed value at the element failure ($D_A = 1$) when the traction-separation curve is complete. To overcome that issue, the proposed model takes the maximum SERR value between its estimation at the element failure and the current estimation value, in a similar way to proposed by Kawashita and Hallett (2012). This approach provides a more stable and accurate SERR value.

For the mixed mode delamination, the Paris's law coefficient and exponent in Eq. (18) are interpolated using the formulation proposed by Blanco et al. (2004).

$$m = m_I + m_b\phi_s + (m_s - m_I - m_b)(\phi_s)^2 \tag{22a}$$

$$\log(C) = \log(C_I) + \log(C_b)\phi_s + \log\left(\frac{C_s}{C_I C_b}\right)(\phi_s)^2 \tag{22b}$$

where ϕ_s is the mode ratio.

$$\phi_s = \frac{J_{II} + J_{II}}{J_I + J_{II} + J_{III}} \tag{23}$$

This formulation presents one fitting parameter for each equation, m_b for the exponent interpolation and C_b for the coefficient interpolation. Therefore, is required leastwise one mixed mode testing data.

With the crack growth rate $\frac{\mathrm{d}a}{\mathrm{d}n}$ obtained from Eqs. (18) to (23), the element fatigue damage rate $\frac{\mathrm{d}D_A^f}{\mathrm{d}n}$ is than calculated applying the chain rule, as given by Eq. (24).

$$\frac{\mathrm{d}D_A^f}{\mathrm{d}n} = \frac{1 - D_A^s}{l_{el}}\frac{\mathrm{d}a}{\mathrm{d}n} \tag{24}$$

where l_{el} is the element length. The fatigue damage parameter is obtained integrating Eq. (24) assuming a constant crack growth rate during the increment,

$$D_A^f(n + \Delta n) = D_A^f(n) + \frac{1 - D_A^s}{l_{el}} C\left[G_{max}\left(1 - R^2\right)\right]^m \Delta n \tag{25}$$

1 MODEL VALIDATION

The proposed model is implemented into Abaqus explicit finite element code through two user subroutines. The local parts of the algorithms, at the element level, are implemented as a material subroutine VUMAT. The non-local parts, such as the J-integral calculation and the tracking crack tip algorithm, needs the information of several elements being implemented in a VEXTERNALDB subroutine.

The model is validated using the experimental data published by Asp, Sjögren and Greenhalgh (2001). The model is tested at three loading conditions simulating the experiment configurations. The mode I fatigue induced simulation model is based on the double-cantilever beam (DCB) configuration, the mode II simulation model is based on the four-point end-notched flexure (4ENF) configuration, and a mixed mode bending (MMB) at $\phi_{II} = 0.5$ configuration is used to test the combined modes. The specimens are made of HTA/6376C carbon/epoxy prepreg with the lay-up $[0_{12}//(\pm 5/0_4)_s]$, where the sign "//" refers to the plane of the artificial delamination. The dimensions are 150*mm* long, 20*mm* wide, with 3.1*mm* thickness, and an initial crack length of 35mm. The laminate properties are given in Table 1. All material properties listed in Table 1 are taken from Asp et al. (2001) except the fitting parameters (λ, C_b and m_b), the interfacial strength (S_I and S_{II}) and interface stiffness (K_I and K_{II}). The interfacial strength for mode II is calculated using the formulation proposed by Turon et al. (2010), given by Eq. (26).

$$S_{II} = S_I\sqrt{\frac{G_{II,c}}{G_{I,c}}} \tag{26}$$

The laminate arms are modelled using 4-node shell elements named S4R while the cohesive zone is modelled with a reduced integration solid hexahedro elements named C3D8R with material behaviour defined by the local subroutine, as shown in Fig. 6. The mesh has 0.1*mm* length at crack growth direction. A rigid tie contact is used to connect the upper and bottom laminate to the cohesive element. In the particular case of the 4ENF test, a single plane rigid element is modelled using R3D4 in order to transfer the load from the actuator to the specimen. A constraint is applied in the element edges at the through-thickness direction connecting the upper laminate to the rigid surface. The maximum loads are applied according to the loading configuration proposed in Robinson et al. (2005) as shown in Fig. 7. The load ration $R = 0.1$ is used (Asp et al., 2001).

Tabela 1 – Mechanical properties (HTA/6376C)

Layer Properties				Interface Properties	
E_{11} (MPa)	$120,000$	$G_{I,c}$ (mJ/mm^2)	0.26	C_I $(mm/cycle)$	2.21×10^{-3}
E_{22} (MPa)	$10,500$	$G_{II,c}$ (mJ/mm^2)	1.002	C_{II} $(mm/cycle)$	1.22×10^{-1}
G_{12} (MPa)	$5,250$	$G_{0.5,c}$ (mJ/mm^2)	0.447	$C_{50\%}$ $(mm/cycle)$	1.68×10^{-1}
G_{13} (MPa)	$5,250$	λ	1.198	C_b	6.09×10^5
$G_{23}(MPa)$	$3,480$	S_I (MPa)	30	m_I	5.09
$\nu_{12} = \nu_{13}$	0.3	S_{II} (MPa)	58.9	m_{II}	4.38
ν_{23}	0.51	K_I (N/mm^3)	1×10^5	$m_{50\%}$	6.28
		K_{II} (N/mm^3)	1×10^5	m_b	5.48

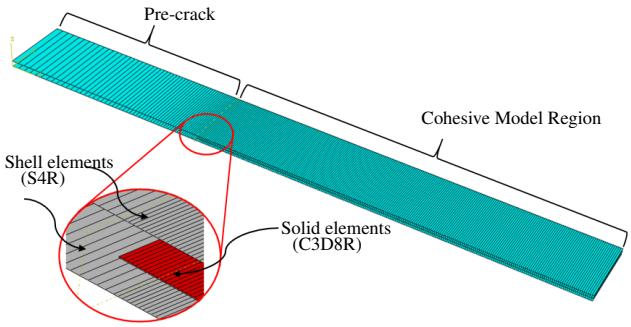

Figura 6 – Coupon mesh detail

RESULTS AND DISCUSSIONS

A traction-separation curve at mode I delamination is presented in Fig. 8. In this analysis, the specimen is loaded at $G_{max} = 0.13mJ/mm^2$, and the results are plotted for the element at $2mm$ ahead the initial crack tip. The SERR is computed at the structure level by the J-integral and, after the element becomes the crack tip, it assumes the maximum value between the current J-integral and value at the neighbour element failure point.

In Fig. 8 can be observed that the traction-separation curve, in black, presents a zero derivative at the on-set point ($\sigma = 30MPa$) followed by the cubic softening curve. After the element becoming the crack tip, it presents a quasi-linear response, which is a combination of stress reduction caused by fatigue damage and the displacement increment resulting from the stiffness degradation. Meanwhile, the SERR presents a stick-slip response as the crack advances through each element. At element fatigue degradation, the maximum value between the current J-integral estimation and its value at the neighbour element failure point results in a predominance of the neighbour value until the element failure.

The results for all three modes ratios are summarised in Fig. 9. This figure shows a comparison between the crack growth rate predicted by the proposed model and the experimental results. For comparative purpose, an equivalent model with a bi-linear TCL is also plotted.

From Fig. 9 it is possible to notice that the proposed model accurately predicts the crack growth rate for all the delamination modes at different SERR levels. The comparison between the bi-linear TSL and linear-polynomial TSL shows that, in addition to the numerical stability, linear-polynomial TSL also presents higher accuracy, mainly for the mixed mode loaded at $0.2G/G_c$

CONCLUSION

A detailed formulation for fatigue-induced delamination modelling in composite laminates and adhesive joints is presented and discussed in this work. The fatigue-driven damage was modelled by combining the static damage with fatigue damage evolution law derived in terms of Paris's Law parameters. The proposed model has been implemented into ABAQUS/Explicit FE within solid elements using two subroutines. The local part (at element level) of the algorithm is implemented in a user-defined material subroutine (VUMAT) and the non-local part (at structure level), in a VEXTER-

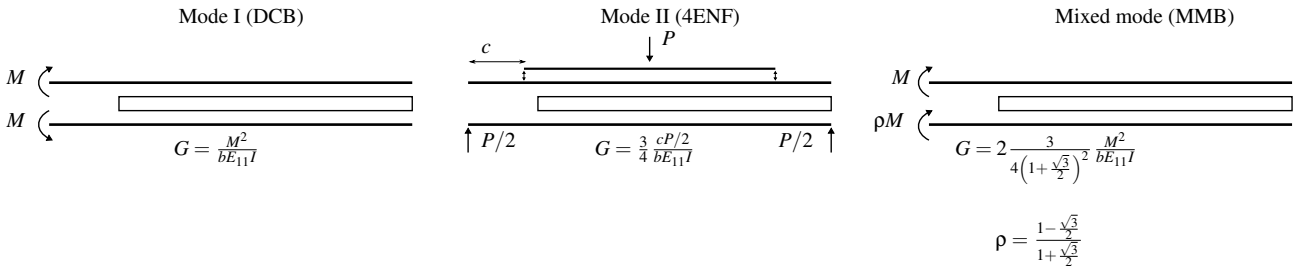

Figura 7 – Loading configurations

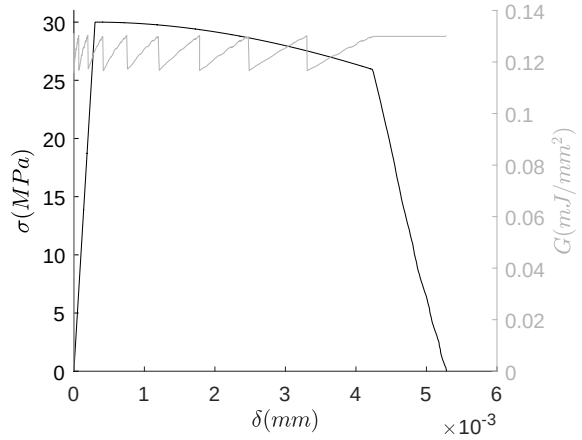

Figura 8 – Traction–separation curve for pure Mode I configuration loaded at $G_{max} = 0.13 mJ/mm^2$.

NALDB subroutine. The proposed model was used to simulate three testing setups and the results were compared with experimental data from the literature. In the simulation tests, the linear-polynomial traction-separation law performed robustly with a good numerical stability and accuracy in terms of energy dissipation. Furthermore, The J-integral enabled accurate predictions of the strain energy ahead of the crack-tip. In addition, the numerical predictions obtained using the proposed model presented a very good correlation with the literature data. The model proposed herein can be easily combined with intralaminar fatigue damage models to predict interaction between intralaminar and interlaminar failure modes. Furthermore, it will integrate a virtual testing platform under development by the Composite Research group at ITA.

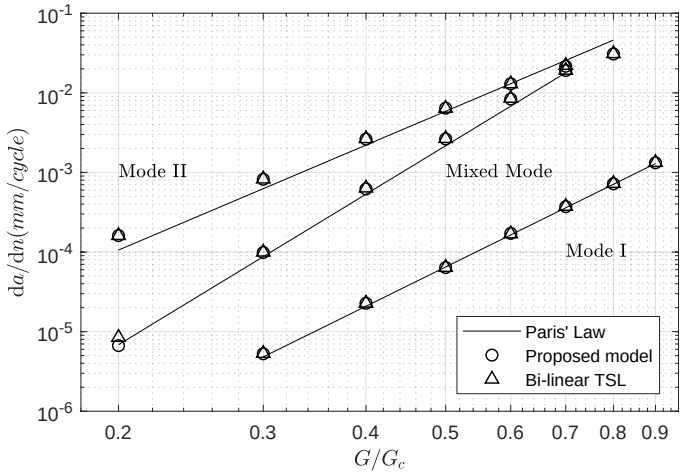

Figura 9 – Comparison between numerical prediction for the crack growth rate and experimental results

ACKNOWLEDGMENTS

The authors acknowledge the financial support received for this work from the national research council CNPq, Grant 301053/2016-2 and 145467/2015-5, FINEP/CAPTAER II, Grant 0109020700 and FAPESP Grant 2015/16733-2.

REFERENCES

Asp, L.E., Sjögren, A. and Greenhalgh, E.S., 2001, "Delamination growth and thresholds in a carbon/epoxy composite under fatigue loading", Journal of Composites, Technology and Research, Vol.23, No. 2, pp. 55–68.

Blanco, N., Gamstedt, E.K., Asp, L.E., Costa, J., 2004, "Mixed-mode delamination growth in carbon-fibre composite laminates under cyclic loading", International Journal of Solids and Structures, Vol. 41, No.15, pp. 4219–4235.

Donadon, M.V. and Lauda, D.P., 2015, "A damage model for the prediction of static and fatigue-driven delamination in composite laminates", Journal of Composite Materials, Vol.49, No. 16, pp. 1995–2007.

Donadon, M.V., De Almeida, S.F.M., Arbelo, M.A. and de Faria, A. R., 2009, "A three-dimensional ply failure model for composite structures", International Journal of Aerospace Engineering, 22 p.

Kawashita, L.F. and Hallett, S.R., 2012 "A crack tip tracking algorithm for cohesive interface element analysis of fatigue delamination propagation in composite materials", International Journal of Solids and Structures, Vol.49, No. 21, pp. 2898–2913.

Peerlings, R.H.J., Brekelmans, W., De Borst, R. and Geers, M.G.D., 2000, "Gradient-enhanced damage modelling of high-cycle fatigue", International Journal for Numerical Methods in Engineering, Vol.49, No. 12, pp. 1547–1569.

Robinson, P., Galvanetto, U., Tumino, D., Bellucci, G. and Violeau, D., 2005, "Numerical simulation of fatigue-driven delamination using interface elements", International Journal for Numerical Methods in Engineering, Vol.63, No. 13, pp. 1824–1848.

Turon, A., Camanho, P.P., Costa, J., and Renart, J., 2010, "Accurate simulation of delamination growth under mixed-mode loading using cohesive elements: Definition of interlaminar strengths and elastic stiffness", Composite Structures, vol. 92 No. 8, pp, 1857–1864.

Turon, A., Costa, J., Camanho, P.P. and Dávila, C.G., 2007, "Simulation of delamination in composites under high-cycle fatigue"Composites Part A: Applied Science and Manufacturing, Vol.38, No. 11, pp. 2270–2282.

Whitcomb, J.D., Langley Research Center, 1984, "Analysis of Instability-related Growth of a Through-width Delamination", NASA technical memorandum. National Aeronautics and Space Administration, Langley Research Center.

Ye, L., 1988, "Role of matrix resin in delamination onset and growth in composite laminates", Composites science and technology, Vol. 33, No. 4, pp. 257–277.

RESPONSIBILITY NOTICE

The author(s) is (are) the only responsible for the printed material included in this paper.